Journal of The Electrochemical Society, **159** (5) A571-A578 (2012)
0013-4651/2012/159(5)/A571/8/$28.00 © The Electrochemical Society

Synthesis and Electrochemical Characterization of $LiNi_{0.8}Co_{0.2}O_2$ as Cathode Material for Aqueous Rechargeable Lithium Batteries

K. C. Mahesh,[a] G. S. Suresh,[a,z] A. J. Bhattacharyya,[b,*] and T. V. Venkatesha[c]

[a] *Chemistry Research Centre, S.S.M.R.V. Degree College, Jayanagar, Bangalore 560041, India*
[b] *Solid State and Structural Chemistry Unit, Indian Institute of Science, Bangalore 560012, India*
[c] *Department of Chemistry, Kuvempu University, Jnanasahyadri, Shankaraghatta-577451, Shimoga, India*

$LiNi_{0.8}Co_{0.2}O_2$ cathode material for lithium ion batteries is synthesized by reaction under autogenic pressure at elevated temperature (RAPET) method. The simple synthesis procedure is time and energy saving, and thus is promising for commercial application. The structure and stability of the material have been characterized by means of XRD and TG-DTA. The electrochemical properties of the $LiNi_{0.8}Co_{0.2}O_2$ cathode are investigated in 2 M Li_2SO_4 aqueous electrolyte and they are compared to that in an organic electrolyte. A battery cell consisting of $LiNi_{0.8}Co_{0.2}O_2$ as cathode in 2 M Li_2SO_4 solution is constructed in combination with $LiTi_2(PO_4)_3$ as anode. The cell retained almost constant discharge capacity over hundred cycles. The electrochemical impedance spectral (EIS) studies in aqueous and nonaqueous electrolytes revealed that the mechanism of lithium ion intercalation and deintercalation processes in $LiNi_{0.8}Co_{0.2}O_2$ electrode follow almost similar mechanism in both aqueous and nonaqueous electrolytes. The chemical diffusion coefficient was calculated from slow scan rate cyclic voltammetry and EIS.
 [DOI: 10.1149/2.075205jes]

Manuscript submitted December 1, 2011; revised manuscript received February 13, 2012. Published March 1, 2012.

The ever increasing demand for portable telecommunication devices, computers and eventually hybrid vehicles has given rise to the increased production of lithium ion rechargeable batteries.[1,2] Sony researchers, who successfully commercialized lithium ion batteries, were the first to develop $LiCoO_2$ as a cathode material. Since then, a tremendous number of studies have been carried out to find the best material, optimize electrochemical properties, and understand the fundamental process involved in the intercalation reactions.[3] Spinel $LiMn_2O_4$ and layered $LiNiO_2$ are alternative cathode materials for lithium ion batteries.[4–6] A tremendous amount of work has been done on these materials. Unfortunately, $LiMn_2O_4$ is still not ready to be used in commercial production due to its short cycle life which is associated with the phase transformation of the spinel during the charge-discharge cycle.[7,8] The poor life time of $LiNiO_2$ over cycling has inhibited the development of lithium ion batteries with this positive electrode material. With respect to practical applications, many works have focused on structural modification and composition optimization to improve the performance of $LiNiO_2$ and its derivatives.[5,6] The substitution of cobalt partially with nickel in the $LiNiO_2$ structure is one of the solution which can lower the cost and improve the reversible capacity of materials. So mixed $LiCo_{1-x}Ni_xO_2$ layered compounds are of great importance as cathode materials for high-energy density lithium ion batteries.[9–11] In a series of papers Delmas group determined the structural details and physical properties of $LiCo_{1-x}Ni_xO_2$ system and showed that there is an increased ordering as the cobalt concentration increases; they found that there is no nickel content on the lithium sites for $x \geq 0.3$.[12–15] Thus cobalt suppresses the migration of nickel to the lithium site in the mixed Li nickel/cobalt oxides.[16]

Over the years, the composition $LiNi_{0.8}Co_{0.2}O_2$ has attracted much attention as a 4 V cathode due to its many advantages compared with $LiCoO_2$, viz., (i) it contains only 20% by mass of toxic cobalt and is cheaper than $LiCoO_2$; (ii) it can be synthesized at a lower temperature (700–800°C) than $LiCoO_2$; (iii) it can give a higher reversible capacity as compared with $LiCoO_2$.[3] The compound exhibits crystal structure phase transitions similar to that of $LiNiO_2$ during charge process due to the de-insertion of lithium ions. As a result, the unit-cell volume change occur that cause retardation of lithium ion intercalation during discharge process which results in capacity fading. This can be reduced to some extent by optimizing the synthesis procedure, by doping with other elements at the cobalt sites, or by coating the surface of the particles with other oxides/compounds. In the charged state, at $x > 0.5$ in $Li_{1-x}Ni_{0.8}Co_{0.2}O_2$, the compound is a strong oxidizing agent due to the presence of Ni^{4+} ions and can slowly cause the decomposition of the liquid electrolyte that results in the evolution of gases. In addition, for $x > 0.5$, the compound is structurally unstable when heated above 200°C and evolves oxygen and decomposition products. Doping at the cobalt sites[17] as well as surface coating by MgO,[18], TiO_2 [19] SiO_x [20] and $AlPO_4$ [3] are some of the strategies employed to reduce or suppress the above effects.

On the other hand, the lithium ion batteries, which offer outstanding technical performances concerning the available gravimetric energy density, are limited by several drawbacks such as the severe safety problems, the economic and environmental problems.[21,22] The flammable organic electrolytes used in lithium ion batteries may cause smoke or fire in the case of improper use such as overcharge or short-circuit. Moreover, lithium ion batteries are expensive, because of the complicated cell designing, the necessity of a perfectly dry environment during some manufacturing steps and the costly nonaqueous electrolytes.[23] Overall, the economic and ecologic problems, with which the present day lithium ion batteries are concerned, continuously urge the development of less expensive and 'green' energy storage materials and devices. As an alternative, a new type of rechargeable lithium ion battery with an aqueous electrolyte was announced in the middle of 1990's.[24–26] This type of battery uses the lithium intercalation compounds as electrode materials and an aqueous electrolyte solution. By this combination, the disadvantages of the non-aqueous lithium battery, i.e. inflammability, toxicity, high cost and safety problems could be avoided. Due to the aqueous electrolyte the cell voltage is restricted to about 1.3 V, the decomposition potential of water, in comparison to 3-4 V in organic electrolyte. As a consequence, only low energy density can be expected from this kind of battery but can be compared with that of Pb-acid and Ni-Cd batteries which uses poisonous metals.

Extensive studies have been devoted to fabricate $LiNi_{0.8}Co_{0.2}O_2$ material through solid state process,[27] sol gel method,[28] co-precipitation route,[29] reverse micro emulsion method,[30] spray drying method etc. Here, we report the use of $LiNi_{0.8}Co_{0.2}O_2$ synthesized by RAPET method as cathode material in combination with $LiTi_2(PO_4)_3$ anode and 2 M Li_2SO_4 aqueous solution as electrolyte. RAPET method is a simple, one-stage, efficient, economic and scalable approach for the synthesis of a variety of materials. The process involves heating of precursors in a closed stainless steel cell. The average particle size and size distribution can be manipulated by controlling the temperature and duration of heating. The electrochemical properties of $LiNi_{0.8}Co_{0.2}O_2$ in an aqueous electrolyte is studied and compared with that in an organic electrolyte.

* Electrochemical Society Active Member.
z E-mail: sureshssmrv@yahoo.co.in

Experimental

Stoichiometric amounts of LiOH, NiO and Co_3O_4 (all from Sigma Aldrich) are weighed to give about 0.6 g product and then mixed and ground well. The resulting powder is introduced into a 5 mL Swagelok. The Swagelok parts consist of a small threaded stainless steel tube closed by two caps from both sides. The filled Swagelok is closed tightly and then placed inside an alumina pipe in the middle of the furnace. The temperature is raised to 600°C at a rate of 10°C/minute and held at this temperature for 14 hours. The chemical dissociation and transformation reaction takes place under the autogenic pressure of the precursor at the fixed temperature. The Swagelok cell is allowed to cool gradually to room temperature, opened and the obtained product is used after grinding. Crystalline $LiTi_2(PO_4)_3$ anode material was prepared in the same way by heating a mixture of TiO_2, $NH_4H_2PO_4$ and LiH_2PO_4 in appropriate molar ratio at 900°C for 15 hours and by cooling it slowly to room temperature.

Powder X-ray diffraction (XRD) patterns of the samples were recorded using a Philips X'pert Pro diffractometer with CuKα ($\lambda = 1.5418A^o$) as the source. Electrodes were prepared by using stainless steel mesh as a current collector. The mesh was cut into circular shape of about 1 cm^2 area and welded with stainless steel wire for electrical contact. The mesh was sandblasted to remove the oxide layer, washed with water, rinsed with acetone, dried and weighed. Cathode and anode materials were prepared in the same way. Powder mixture of the sample, carbon black and polytetafluoroethylene (PTFE) in the weight ratio 80:10:10 were ground in a mortar; a few drops of NMP were added to get slurry. The slurry was coated onto the pretreated mesh and dried in a vacuum oven at 110°C overnight.

A three electrode electrochemical cell was employed for cyclic voltammetry (CV) in aqueous 2 M Li_2SO_4 solution. A saturated calomel electrode (SCE) and Pt foil were used as reference and counter electrodes respectively. Galvanostatic charge-discharge measurements were carried out using coin-type cell consisting of $LiNi_{0.8}Co_{0.2}O_2$ cathode and $LiTi_2(PO_4)_3$ anode. Electrochemical impedance measurements were carried out potentiometrically using a three electrode system with an ac excitation signal of 10 mV over the frequency range from 100 kHz to 5 mHz. All the experiments of $LiNi_{0.8}Co_{0.2}O_2$ in organic electrolyte were carried out in the same way. The test cell was prepared with Li metal foil as reference and counter electrodes, and a 1 M $LiAsF_6$ dissolved in EC+DMC (1:1 v/v) as the electrolyte solution. Celgard 2340 was used as the separator. Assembling of the cell was carried out in a glove box filled with argon gas. All the electrochemical measurements were made using a Biologic potentiostat - galvanostat instrument.

Results and Discussion

Physical characterization.— The structure of $LiNi_{0.8}Co_{0.2}O_2$ is based on a nearly perfect cubic close packing of oxygen atoms, with the small lithium and transition metal atoms occupying alternate layers in the octahedral interstices of the oxygen array, forming a face centered cubic structure. Each cation has six oxygen neighbors and each oxygen has three lithium neighbors and three nickel/cobalt neighbors. Thus, this structure assumes a hexagonal symmetry with an (. . . O – Li – O – Ni – O – Li – O –Ni – O . . .) basal plane stacking sequence. In this structure, the hexagonal *c*-axis corresponds to the body diagonal through the cubic unit cells.[31] The XRD pattern of $LiNi_{0.8}Co_{0.2}O_2$ compound prepared by RAPET method at 600°C for 14 h and solid state method at 800°C for 24 h are shown in Figure 1a. The pattern can be indexed to a single phase of the α-$NaFeO_2$ type with space group *R*3*m* and show very sharp peaks, indicating a high degree of crystallinity. The largest peak at about $2\theta = 18^\circ$ is assigned to the diffraction at the (003) plane indicating the layered structure of $LiNi_{0.8}Co_{0.2}O_2$. The diffraction peaks show a clear splitting of the hexagonal characteristic doublets (006)/(102) and (108)/(110), indicating that the product has the typical layered characteristic. The low values of *R* factor, $R = (I_{102}+I_{006})/I_{101}$, relates to the integrated intensities of the corresponding well resolved peaks of the material

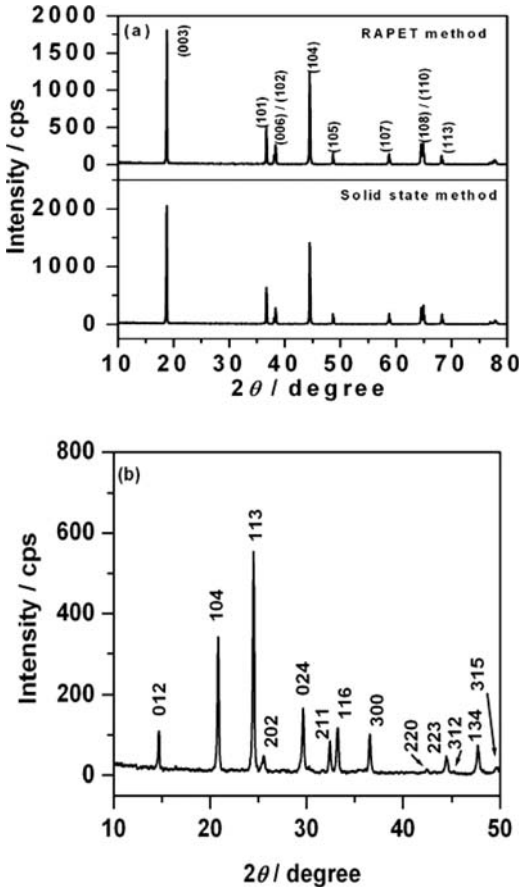

Figure 1. XRD pattern of (a) $LiNi_{0.8}Co_{0.2}O_2$ synthesized by solid state and RAPET methods. (b) $LiTi_2(PO_4)_3$ synthesized by RAPET method.

confirm their hexagonal ordering. The lower the *R*-factor, the better is hexagonal ordering. The ratios of the intensities of 003 and 104 peaks in the XRD pattern, was found to be >1. This indicates no pronounced cation mixing and thereby the electrochemical activity of these cathode materials in terms of capacity and rates of lithium ion de-insertion/insertion is to be very good. We conclude from this XRD results that there are no remarkable impurities in the material obtained and Co^{3+} and Ni^{3+} ions are compatible in the layered hexagonal structure and pure phase solid solutions were obtained. Figure 1b shows the XRD patterns of the $LiTi_2(PO_4)_3$ material synthesized by RAPET method. The sample prepared was phase pure according to the XRD pattern. The XRD peaks can be indexed in the rhombohedral crystal system (space group *R*3*c*).

Thermal stability.— Thermal analysis of the prepared $LiNi_{0.8}Co_{0.2}O_2$ material was performed. TG and DTA traces by thermal analysis of the powders obtained by RAPET method are shown in Figure 2. The sample was heated at 10°C / minute up to 800°C. On TGA curve, about 6% weight loss is observed when the sample is heated up to 500°C. Accordingly a broad endothermic peak is obtained on DTA curve. Between 500–650°C, the weight of the sample hardly changes. It mainly associates the $LiNi_{0.8}Co_{0.2}O_2$ crystallization. The weight loss of the compound above 650°C can be attributed to the extraction of oxygen from the structure according to the following reaction.[10]

$$(1+x)\,LiNi_{0.8}Co_{0.2}O_2 \rightarrow Li_{1-x}(Ni_{0.8}Co_{0.2})_{1+x}O_2 + x\,Li_2O + x/2\,O_2 \quad [1]$$

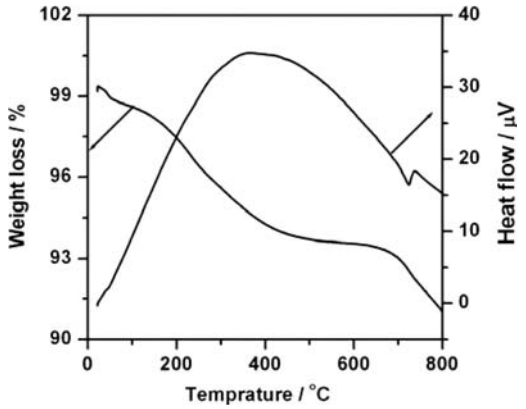

Figure 2. TG - DTA profile of $LiNi_{0.8}Co_{0.2}O_2$ material.

Cyclic voltammetry.— The Cyclic voltammogram of $LiNi_{0.8}Co_{0.2}O_2$ prepared by RAPET method in 2 M Li_2SO_4 aqueous solution at a scan rate of 0.1 mV s^{-1} between 0.0 and 1.0 V using saturated calomel as reference electrode (SCE) is shown in Figure 3a. $LiNi_{0.8}Co_{0.2}O_2$ exhibits one large pair of anodic and cathodic peaks located at 0.65/0.63 V and two small reversible anodic and cathodic peaks at approximately 0.83/0.80 and 0.92/0.89 V, corresponding to lithium intercalation and de-intercalation of $LiNi_{0.8}Co_{0.2}O_2$ electrode in accordance with the following equations.

$$\text{Deintercalation} : LiNi_{0.8}Co_{0.2}O_2 \rightarrow Li_{1-x}Ni_{0.8}Co_{0.2}O_2 + xLi^+ + xe^- \ (x < 1, \text{ at about } 0.65 \text{ V}) \quad [2]$$

$$\text{Intercalation} : Li_{1-x}Ni_{0.8}Co_{0.2}O_2 + xLi^+ + xe^- \rightarrow LiNi_{0.8}Co_{0.2}O_2 \ (x < 1, \text{ at about } 0.63 \text{ V}) \quad [3]$$

The anodic peaks appear due to the oxidation of cobalt and nickel ions accompanied by the deintercalation of equal number of lithium ions. The cathodic peaks are due to the reduction of cobalt and nickel ions accompanied by the intercalation of lithium ions. The first redox couple at 0.65/0.63 is related to the existence of a two-phase domain of $Li_xNi_{0.8}Co_{0.2}O_2$; the two small pairs of redox peaks at 0.83/0.80 and 0.92/0.89 V correspond to the presence of a distortion due to an interslab lithium/vacancy ordering.[32] These measurements indicate a sequence of three distinct phase changes occurring as the value of x is electrochemically varied between 1 and 0.4. During these processes, no oxygen evolution peak can be observed, which is obviously due to the over potential of the electrode. To prove the redox reactions of $LiNi_{0.8}Co_{0.2}O_2$ cathode corresponding to lithium ion intercalation-deintercalation, CV performance of the electrode in 2 M Li_2SO_4 aqueous solutions without active material were also investigated. No side reactions were observed except for evolution peak of oxygen. This shows that it is possible to remove lithium ions from the material before the evolution of oxygen. Thus it is possible to use the prepared $LiNi_{0.8}Co_{0.2}O_2$ as cathode material in the aqueous solution without much oxygen evolution.

Figure 3b shows the CV profile of $LiNi_{0.8}Co_{0.2}O_2$ obtained in the organic electrolyte at a scan rate of 0.05 mV s^{-1} using lithium foil as counter and reference electrodes. The cell was cycled in the range from 3.2 to 4.3 V (vs. Li / Li^+). A pair of redox peaks at 4.00 and 3.84 V which correspond to the lithium ion de-intercalation/ intercalation are observed. It can be seen clearly that in the non-aqueous solution the current response of the redox reaction is much lower than that in the aqueous electrolyte solution due to the low ionic conductivity of organic-based solutions. The solvation of lithium ions in the organic solvent with high dipole moment and the resistance offered

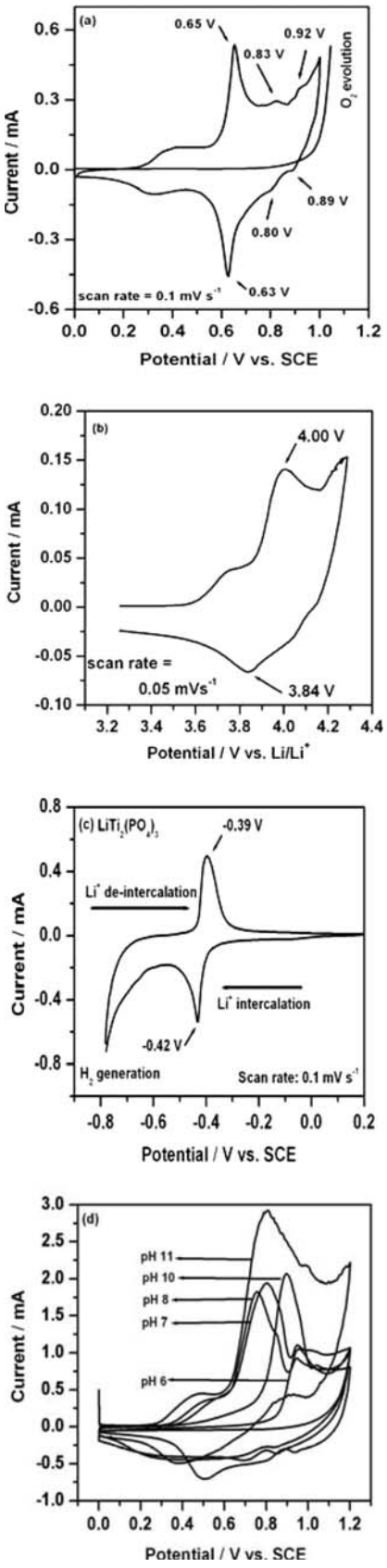

Figure 3. CV of $LiNi_{0.8}Co_{0.2}O_2$ electrode in (a) 2 M Li_2SO_4 aqueous electrolyte (scan rate = 0.1 mVs^{-1}). CV of active material-free electrode is also shown (b) 1 M $LiAsF_6$ / EC+DMC (scan rate = 0.05 mVs^{-1}). (c) CV of $LiTi_2(PO_4)_3$ electrode in 2 M Li_2SO_4 (scan rate = 0.1 mVs^{-1}) (d) CV of $LiNi_{0.8}Co_{0.2}O_2$ electrode in 2 M Li_2SO_4 aqueous electrolyte at different pH.

by the surface layer for lithium ion migration will have a retardation effect on the kinetics of lithium ion insertion. Furthermore, it can be seen that the electrode polarization increases significantly in the organic electrolyte so that the shoulder-like peaks overlap with each other and are less pronounced. In the aqueous solution the smaller peaks appear due to the low electrode polarization.

Figure 3c shows the CV of $LiTi_2(PO_4)_3$ anode in 2 M Li2SO_4 at a scan rate of 0.1 mVs^{-1}. $LiTi_2(PO_4)_3$ exhibits lithium intercalation and de-intercalation potentials of −0.42 V and −0.39 V respectively. Since hydrogen evolution was observed at a more negative potential, it becomes clear that $LiTi_2(PO_4)_3$ can be used as anode in combination with $LiNi_{0.8}Co_{0.2}O_2$ cathode in aqueous electrolyte solutions without much hydrogen evolution.

Figure 3d shows the cyclic voltammograms of $LiNi_{0.8}Co_{0.2}O_2$ electrodes in 2 M Li_2SO_4 aqueous electrolytes recorded at different pH ranging from 6 to 11. The electrolyte pH was adjusted by adding various amounts of 0.1 M H_3BO_3 and 0.1 M LiOH. Generally all the voltammograms are dominated by one single cathodic and anodic peak, regardless of electrolyte pH. These two peaks correspond to the lithium intercalation and deintercalation reactions as discussed earlier. The differences in voltammograms obtained at different pH manifest themselves primarily in the shape of cathodic and anodic peaks as well as the current obtained. At lower and higher pH (<7 and >10), the peaks are spread over a large potential and are broadened. The anodic current increases sharply at higher pH. This appears to reflect the larger influence of oxygen evolution at higher pH. Hence the possibility of oxygen evolution is enhanced and consequently more interaction between oxygen evolution and the lithium intercalation and deintercalation reactions would be expected at higher pH. When the electrode is cycled higher and lower pH the reduction peak does not appear clearly. As voltammograms with clear anodic and cathodic peaks were obtained in 2 M Li_2SO_4 of pH 8, the rest of the experiments were conducted in this solution.

To identify whether the cation deintercalated/intercalated from /into $LiNi_{0.8}Co_{0.2}O_2$ is lithium ion or not, we have recorded the CVs of the electrode at different concentrations of Li_2SO_4 aqueous electrolytes. Figure 4a shows the cyclic voltammograms of $LiNi_{0.8}Co_{0.2}O_2$ electrode with a scan rate of 0.1 mV s^{-1} in various concentrations of Li_2SO_4 aqueous electrolytes. If we suppose that the deintercalating-intercalating cation is lithium ion, then equation 23 represent the corresponding reactions. In accordance with these reactions one should, according to Nernst, observe the following dependence of the formal potential, $E_f = (E_a + E_c)/2$ (where E_a and E_c are the anodic and cathodic peak potentials respectively) on activity of the alkali cation:

$$E_f = E^\circ + \log a_{Li+} \quad [4]$$

i.e., the formal potential of the redox reaction should be directly proportional to the logarithm of lithium ion activity in the Li_2SO_4 electrolyte solution. Figure 4b shows the plot of E_f vs. log [Li^+] at various concentrations of alkali electrolyte solutions. The straight line with a positive slope confirms that, the redox peaks on the CVs of $LiNi_{0.8}Co_{0.2}O_2$ in Li_2SO_4 aqueous electrolytes can be attributed to the deintercalation-intercalation of lithium ions.

CVs of $LiNi_{0.8}Co_{0.2}O_2$ at different scan rates from 0.1 to 0.9 mV s^{-1} in 2 M Li_2SO_4 solution are shown in Figure 5a. It can be seen clearly that the electrode polarization increases significantly as the scan rate increases, and the three couples of redox peaks overlapped with each other and are less pronounced. Although, the curve shape of the anodic and cathodic peaks was almost symmetrical, the peak potential difference between the two peaks is increased with increase in scan rate. The reversibility of lithium ion intercalation-deintercalation depends on scan rate. At low scan rates, the system may yield reversible waves, while at large scan rates, irreversible behavior is observed, which may make us assume that the electrochemical lithium ion deintercalation-intercalation process changes from being kinetically quasi-reversible to irreversible when scanning rate increases from low to high.[33] Nevertheless, the redox peaks at low scan rate are better defined than that at medium rate, because the lithium ions cannot completely

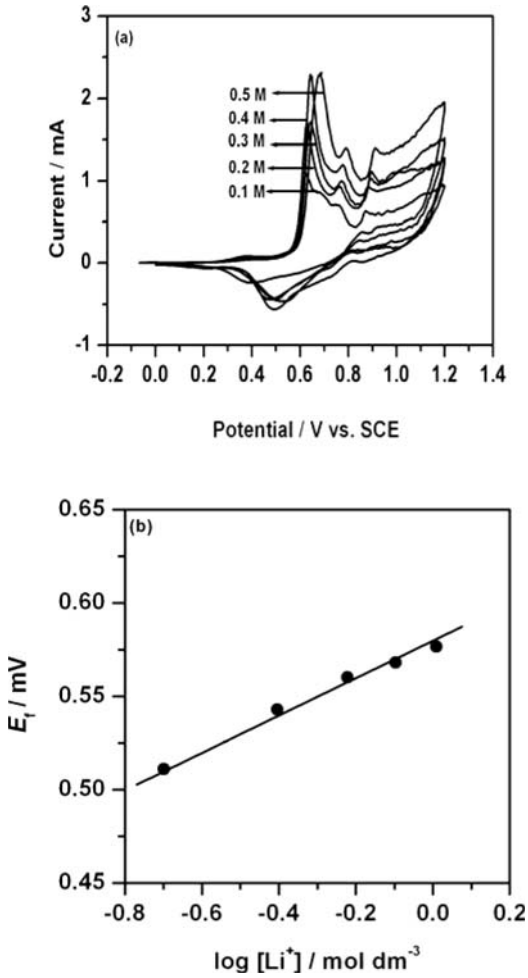

Figure 4. (a) CV of $LiNi_{0.8}Co_{0.2}O_2$ electrode at a scan rate of 0.1 mVs^{-1} at different concentrations of Li_2SO_4 electrolyte. (b) Plot of E_f vs. log [Li^+] in Li_2SO_4 electrolytes.

extract/insert from/into the bulk of the electrode during the time interval of a high scan rate. The anodic and cathodic peak currents ($i_{p,a}$ and $i_{p,c}$) from Figure 5a as the function of square root of scan rates are shown in Figure 5b. It can be seen that there is a linear relationship between the peak current and the square root of scan rate, which means that the lithium intercalation-deintercalation process in the compound is diffusion controlled.

Figure 5c shows scan rate dependency of the cathodic and anodic peak separation obtained from cyclic voltammograms of $LiNi_{0.8}Co_{0.2}O_2$ electrode in 2 M Li_2SO_4 at different scan rates. As expected, the peak separation increases with increase in scan rate as the anodic peaks shift toward a more positive potential and cathodic peaks shift to the negative ones. This could be ascribed to the effect of concentration polarization and may be due to slow electron transfer.[34] The contribution of *i*R-drop to this behavior is negligibly small as the ionic conductivity of the aqueous Li_2SO_4 solution is very high.

As the kinetics of a solid-state diffusion process limit the total reaction rate, diffusion coefficient is one of the most important kinetic parameters for ion-insertion compounds. It also is very important in battery application as the total reaction rate is related to the maximum current of the battery. However, the electrochemical lithium intercalation-deintercalation reaction is diffusion limited. Hence, chemical diffusion coefficients of lithium ions were roughly estimated by cyclic voltammetry. In linear potential sweep voltammograms of a reversible system the peak current (I_p in amperes)

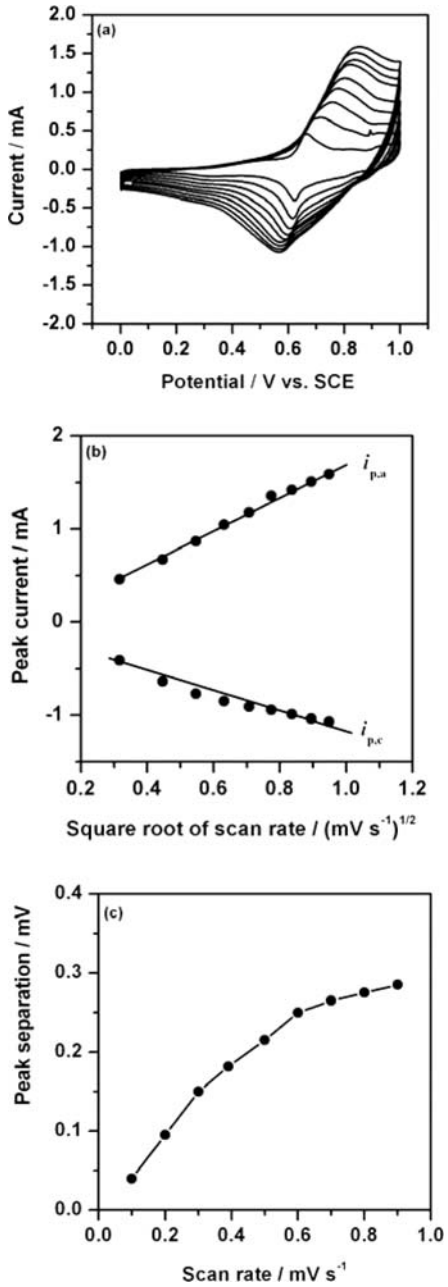

Figure 5. (a) CV of $LiNi_{0.8}Co_{0.2}O_2$ electrode 2 M Li_2SO_4 at different scan rates. (b) Relationship between the peak currents and square root of scan rate in 2 M Li_2SO_4 at different scan rates. (c) Effect of scan rate on the peak separation.

is given by [35]

$$I_p = 2.69 \times 10^5 A n^{2/3} C D^{1/2} \nu^{1/2} \quad (\text{at } 25^\circ\text{C}). \qquad [5]$$

where, A is the surface area of the cathode (geometric surface area of the electrode is used instead), n is the number of the electrons transferred during intercalation, C is the concentration of lithium ions, D is the chemical diffusion coefficient of lithium ions, and ν is the san rate. Cyclic voltammograms at scan rates of 0.1 to 0.9 mV s^{-1} in Figure 5a are used to calculate lithium ion diffusion coefficient. The corresponding D values are listed in Table I. The values are in the order of 10^{-9} cm^2 s^{-1}, which is slightly larger than that of $LiNi_{0.8}Co_{0.2}O_2$ in nonaqueous electrolyte determined by PITT and GITT.[36] The larger value of diffusion coefficient may be because of the smaller particle size of the prepared compound and the lower viscosity

Table I. Diffusion coefficient, D calculated from the anodic and cathodic peak currents of CV profiles at different scan rates.

Scan rate/ mV s^{-1}	D (anodic)/ $\times 10^{-9}$ cm^2 s^{-1}	D (cathodic)/ $\times 10^{-9}$ cm^2 s^{-1}
0.1	2.354	1.853
0.2	2.504	2.248
0.3	2.795	2.195
0.4	3.035	2.000
0.5	3.080	1.827
0.6	3.405	1.649
0.7	3.182	1.554
0.8	3.157	1.489
0.9	3.116	1.415

of the aqueous electrolytes. Further, linear sweep voltammetry can provide only effective or average values of diffusion coefficient related to the potential range around the voltammetric peak.

Galvanostatic Charge-discharge cycling.— The charging and discharging of lithium ion batteries involves lithium ion transfer from one insertion electrode to another one. This transfer can be considered as a topotactic intercalation reaction, meaning that the guest ions occupy the interstitial sites of both crystalline host matrices and that their charging and discharging result in a nonuniform concentration profile in the electrodes' bulk, thus separating the coexisting phases with different concentrations of guest ions. The coexistence of different phases during intercalation has been confirmed by in situ XRD characterizations for a large variety of ion insertion electrodes. The process of ion insertion into host electrodes that have been polarized in solutions can be regarded as first order phase transition.[37]

To study the charge discharge cycling behavior of the prepared $LiNi_{0.8}Co_{0.2}O_2$ electrodes, an electrochemical cell was constructed using $LiNi_{0.8}Co_{0.2}O_2$ as cathode and $LiTi_2(PO_4)_3$ as anode in 2 M Li_2SO_4 aqueous solution. The charge and discharge curves of $LiTi_2(PO_4)_3$ / 2 M Li_2SO_4 / $LiNi_{0.8}Co_{0.2}O_2$ cell at a current density of 0.1 mA cm^{-2} are shown in Figure 6a. The voltage range was limited between 0 and 1.3 V. It is clear that lithium ions deintercalate from $LiNi_{0.8}Co_{0.2}O_2$ and intercalate into $LiTi_2(PO_4)_3$ during the charge process and during discharge the opposite process occurs, i.e., lithium ions deintercalate from $LiTi_2(PO_4)_3$ and intercalate into $LiNi_{0.8}Co_{0.2}O_2$ in accordance with the following equations:

$$\text{Charge}: \ LiNi_{0.8}Co_{0.2}O_2 + LiTi_2(PO_4)_3 \rightarrow Li_{(1-x)}Ni_{0.8}Co_{0.2}O_2 + Li_{(1+x)}Ti_2(PO_4)_3 \qquad [6]$$

$$\text{Discharge}: \ Li_{(1-x)}Ni_{0.8}Co_{0.2}O_2 + Li_{(1+x)}Ti_2(PO_4)_3 \rightarrow LiNi_{0.8}Co_{0.2}O_2 + LiTi_2(PO_4)_3 \qquad [7]$$

In the first cycle, the charge and discharge capacities are 65 and 63 mAh g^{-1} based on the weight of the electrodes, and the coulombic efficiency is 96%. The sloping behavior of the charge-discharge curves observed is reported to be due to the presence of amorphous phase in the cathode material. These curves are almost similar in shape and diplay a voltage plateau of about 0.8 V. This shows that output voltage of the $LiTi_2(PO_4)_3$ / 2 M Li_2SO_4 / $LiNi_{0.8}Co_{0.2}O_2$ cell is comparable to those of Ni-MH and Ni-Cd cells. In fact the capacity is greater than that of Ni-Cd cells. If further study is carried out and the capacity of the cathode is increased, it is possible to reach the level of Ni-MH systems. Apparently, there is no evident capacity fading during the first 100 cycles. This can be ascribed to the good stability of the two electrodes during cycling in the aqueous electrolyte and shows that this kind of cell is good in reversible intercalation and deintercalation of lithium ions. The good cycling performance could be attributed to the high

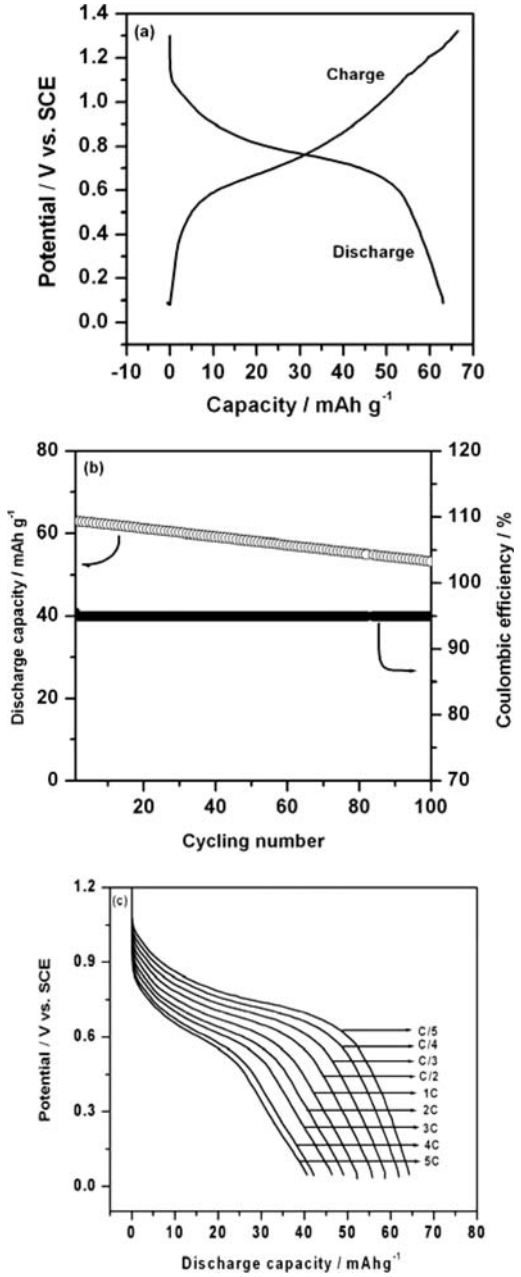

Figure 6. (a) Charge-discharge curves (b) cycling behavior at a current density of 0.1 mA cm^{-2} (c) discharge curves at different C_{rates} of $LiTi_2(PO_4)_3$/ $LiNi_{0.8}Co_{0.2}O_2$ cell in 2 M Li_2SO_4 electrolyte.

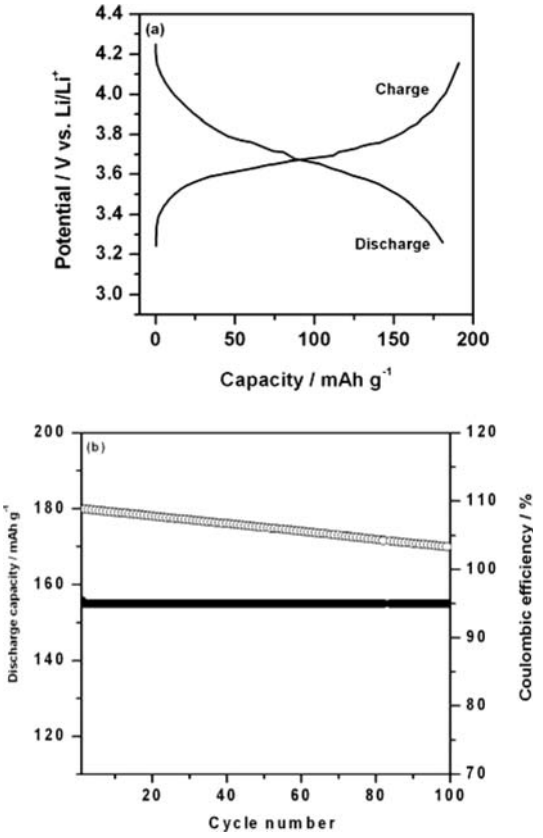

Figure 7. (a) Charge and discharge curves (b) cycling behavior at a current density of 0.1 mA cm^{-2} of Li/ / $LiNi_{0.8}Co_{0.2}O_2$ cell in nonaqueous electrolyte.

phase purity, small particle distribution and improved conductivity of the prepared materials. The porous structure ensures the effective ingress of the electrolyte, and the small particle character reduces the diffusion length of the lithium ion inside, which results in fast reaction and diffusion kinetics. It is well known that the electrode material with high surface area and small particle size increases the rate capability of the lithium ion batteries. The variation of discharge capacity and coulombic efficiency with cycle number is shown in Figure 6b. After hundred cycles, the charge-discharge efficiency, which is the ratio of the discharge capacity to that of the charge capacity for a given cycle, is more than 95%. This value indicates that almost the complete deintercalated amount of lithium ions can be intercalated during the succeeding discharge process. The discharge curves of the above cell at different discharge rates ranging from C/5 to 5 C are as shown in Figure 6c. The cell delivers a discharge capacity of 65 mAh g^{-1} at C/5 rate and 40 mAh g^{-1} at 5 C rate. The high-rate discharge performance indicates that the synthesized $LiNi_{0.8}Co_{0.2}O_2$ material is suited for electrode materials of high-power lithium batteries.

Figure 7a shows the charge-discharge and cycling stability curves of Li/ 1 M $LiAsF_6$ / EC+DMC / $LiNi_{0.8}Co_{0.2}O_2$ cell at the current density of 0.1 mA cm^{-2} in the potential range 3.2 to 4.3 V. The curves are similar to that in aqueous electrolyte except that the capacity in the former is lower than that in the latter. This is due to the lower potential window of aqueous electrolytes. These results clearly show that the charge and discharge behavior in organic electrolytes can be transferred into aqueous solution if the intercalation and de-intercalation voltages are within the stable electrochemical window of water.

Electrochemical impedance studies.— The further information about the mechanism of intercalation-deintercalation process of $LiNi_{0.8}Co_{0.2}O_2$ electrode was obtained by electrochemical impedance spectroscopy. Figures 8a–8c shows a family of Nyquist plots related to lithium ion de-intercalation from $LiNi_{0.8}Co_{0.2}O_2$ electrode in 2 M Li_2SO_4 aqueous solution in the potential range 0.1 to 1.1 V. Quantitatively all the spectra can be distinguished in these sections: a potential dependent semicircle in the high frequency region, a Warburg type element in the middle to low frequency region (straight line with 45° angle to Z' axis) and a sloping line at the lower frequencies. These impedance spectra reflect the nature of overall lithium ion de-intercalation process. The high frequency semicircle is related to charge transfer through the electrode/electrolyte interface, the Warburg region is assigned to the diffusion of lithium ions through the bulk electrolyte, while the sloping line reflects a capacitive behavior of the electrode.[38] In accordance with the results obtained an equivalent circuit, as shown in Figure 8d, is proposed to fit the impedance spectra. In this equivalent circuit R_s represents the ohmic resistance of the electrolyte solution which is related to the distance of the high

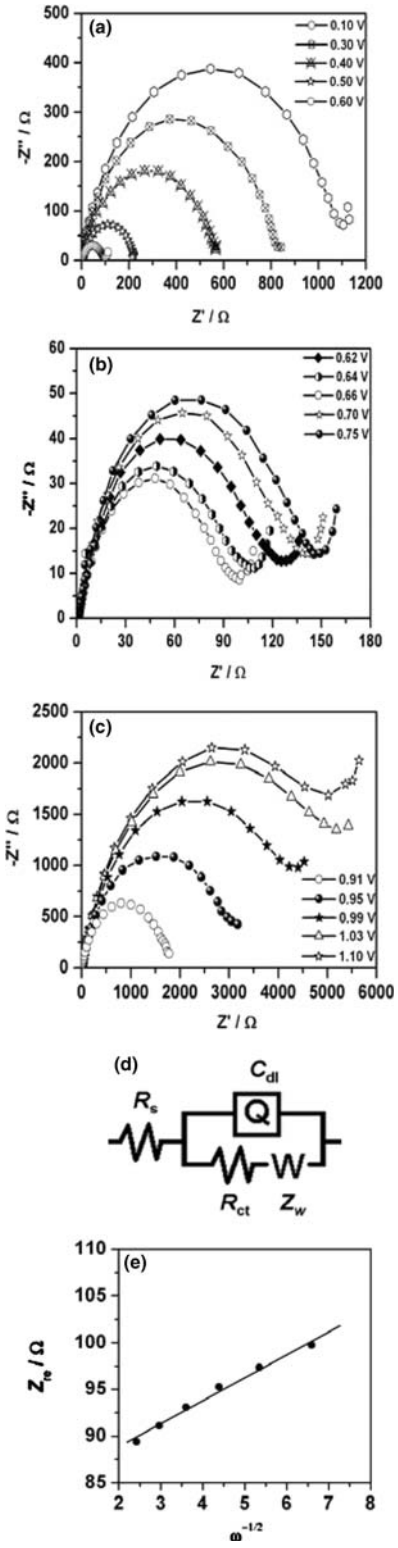

Figure 8. (a)-(c) Nyquist plots of the $LiNi_{0.8}Co_{0.2}O_2$ electrode in 2 M Li_2SO_4 at different charge voltages. (d) corresponding equivalent circuit. (e) Plot of real part of impedance spectra in Figure 8b vs. the square root of frequency.

frequency intercept with the real axis to the axis origin, R_{ct} is the resistance of the charge transfer reaction, Q is the capacitance of the electrode- electrolyte double layer and Z_w is the Warburg impedance. To get better fitting results pure capacitor in the equivalent circuit is replaced by constant phase element (CPE, Q). CPE is used when impedance spectra exhibits low frequency dispersion. It is suggested that such dispersion could be caused by the film- substrate interface, roughness, porosity or in homogeneity.[39] A Nyquist plot of similar compounds in non aqueous electrolytes consists of two semicircles: a potential independent semicircle in the high frequency region and a strongly potential dependent larger semicircle in the medium frequency region.[40] The high frequency semicircle reflects the resistance for lithium ion migration through the surface film and film capacitance of the electrode. The absence of this region may be due to high rate performance (short diffusion path) and/or a small resistance offered by the surface layer for the migration of lithium ions which does not resist the diffusion of lithium ions.

Figure 8a shows a family of Nyquist plots related to lithium ion deintercalation into the layered phase before the CV peak potential. In these curves the diameters of the semicircle decreases with the increase in potential, indicating that the charge transfer resistance and the interfacial capacitance between the electrode and the electrolyte decreases with the increase in potential. Figure 8b shows the Nyquist plots in the vicinity of CV peak potentials. The diameter of the curve decreases further with the appearance of a Warburg region which corresponds to the diffusion of lithium ions through the electrode. In this region the impedance spectra shows minima with respect to $-Z''$ values with comparable diameters. In this figure, we see a curve at 0.66 V with a minimum diameter. The potential of the above minimum almost corresponds to the potential of the CV peak. There after the diameter increases. The minimum diameter and the lowest R_{ct} indicate the favorable kinetic conditions for lithium ion deintercalation at the potential corresponding to the CV peak. Figure 8c shows the impedance spectra measured at potentials after the CV peak, i.e. toward the end of lithium deintercalation process. The diameter of the semicircle increases as the potential becomes more positive. Moreover the capacitive line begins to appear indicating the end of lithium ion deintercalation.

The diffusion coefficient of lithium ions can be calculated from the Nyquist plots in the low frequency region according to the following equation.[35]

$$D = R^2T^2/2A^2n^4F^4C^2\sigma^2 \quad [8]$$

where R is the gas constant, T is the absolute temperature, n is the number of the electrons, A is the surface area, F is Faraday constant, C is concentration, and σ is the Warburg factor which is related to the real part of impedance (Z_{re}) as

$$Z_{re} = R_s + R_{ct} + \omega^{-1/2} \quad [9]$$

where ω is the angular frequency of the small-amplitude ac voltage. Figure 8e shows the relationship between Z_{re} and $\omega^{-1/2}$ in the low frequency region of Nyquist plots in Figure 8b. As expected, a straight line with positive slope is obtained in accordance with the equation 9. The variation of log D, calculated using equation 8, with the potential during the lithium ion intercalation process is shown in Figure 9. One can see that the potential of minima on the log D versus E correspond well with the potential of anodic CV peak as expected. As already reported, in accordance with the view on the influence of short-range interactions on lithium ion diffusion, log D versus E plots calculated from many lithium insertion electrodes have sharp minima at the slow scan rate CV peak potentials.[41,42]

We have recorded the Nyquist plots from the $LiNi_{0.8}Co_{0.2}O_2$ electrode in the organic electrolyte at different applied potentials during the charge process (Figure not shown). The plots consist of two semicircles-an arc like potential independent semicircle in the high frequency region and a strongly potential dependent larger semicircle in the medium frequency region. The high frequency semicircle reflects the resistance for lithium ion migration through the surface film and film capacitance of the electrode. The absence of this region in aqueous electrolytes implies that the electrode surface is not covered with the resistive film and hence migration of lithium ion through the surface film is no longer the necessary stage in the overall lithium intercalation/deintercalation process.[43] Moreover, the low value for R_{ct} in aqueous solution compared to that in nonaqueous solution is also attributed to the absence of surface film formation in aqueous systems.

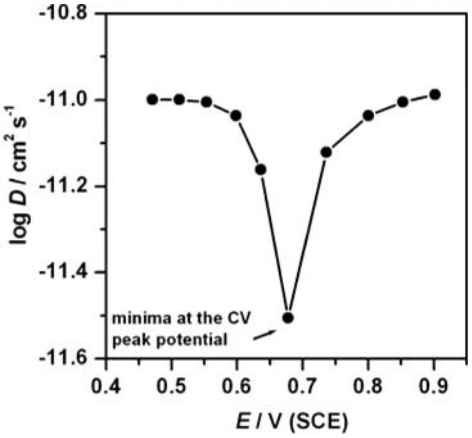

Figure 9. Plot of log*D* vs. *E* obtained from EIS techniques in 2 M Li_2SO_4 at different charge voltages.

It is known that the charge transfer reaction significantly depends on the resistance of the surface film. Hence the absence of surface film enhances the charge transfer kinetics in aqueous electrolytes.

Conclusions

$LiNi_{0.8}Co_{0.2}O_2$ cathode materials were synthesized by a simple, time and energy saving method called RAPET. CV measurements show that the electrode is stable in both aqueous and nonaqueous electrolytes. An aqueous rechargeable lithium battery, $LiTi_2(PO_4)_3$/2 M Li_2SO_4/ $LiNi_{0.8}Co_{0.2}O_2$, has been constructed based on intercalation and de-intercalation of lithium ions during charge and discharge process and it is compared with that in a non aqueous solution. Better cycling behavior was observed due to good reversibility of intercalation and de-intercalation of lithium ions. Slow scan rate CV and EIS studies reveal that the diffusion coefficient of lithium ions in both aqueous and non aqueous electrolytes is similar.

Acknowledgments

The authors gratefully acknowledge the financial support from the Department of Science and Technology, Government of India. Authors thank Sri. A. V. S. Murthy, honorary secretary, Rashtreeya Sikshana Samiti Trust, Bangalore and Dr. P. Yashoda, Principal, S.S.M.R.V. Degree College, Bangalore for their support and encouragement. Authors thank the department of Chemistry, St. Joseph's College for XRD data.

References

1. J. M. Tarscon and M. Armand, *Nature*, **414**, 359 (2001).
2. H. Manjunatha, G. S. Suresh, and T. V. Venkatesha, *J. Solid State Electrochem.*, **15**, 431 (2010).
3. M. H. Kim, H. S. Shin, D. Shin, and Y. K. Sun, *J. Power Sources*, **159**, 1328 (2006).
4. H. Manjunatha, K. C. Mahesh, G. S. Suresh, and T. V. Venkatesha, *Electrochim. Acta*, **56**, 1439 (2011).
5. M. R. Palacin, D. Larcher, A. Audemer, N. Sac-Epee, G. G. Amatucci, and J. M. Tarascon, *J. Electrochem. Soc.*, **144**, 4226 (1997).
6. M. Takno, R. Kanno, and T. Takeda, *Mater. Sci. Eng. B*, **63**, 6 (1999).
7. G. G. Amatuci and A. Blyr, *Solid State Ionics*, **104**, 13 (1997).
8. F. K. Shokoohi, J. M. Tarascon, and B. J. Wikens, *Appl. Phys. Lett.*, **59**, 1260 (1991).
9. J. Molenda, P. Wilk, and J. Marzec, *Solid State Ionics*, **119**, 19 (1999).
10. G. X. Wang, J. Horvat, D. H. Bradhurst, H. K. Liu, and S. X. Dou, *J. Power Sources*, **85**, 279 (2000).
11. Y. Tao, Z. Chen, and B. Zhu, *Solid State Ionics*, **176**, 57 (2005).
12. A. Rougier, I. Saadouane, P. Gravereau, P. Willmann, and C. Delmas, *Solid State Ionics*, **90**, 83 (1996).
13. I. Saadouane and C. Delmas, *J. Solid State Chem.*, **136**, 8 (1998).
14. I. Saadouane, M. Menetrier, and C. Delmas, *J. Mater. Chem.*, **7**, 2505 (1997).
15. I. Saadouane and C. Delmas, *J. Mater. Chem.*, **6**, 193 (1996).
16. M. S. Whittingham, *Chem. Rev.*, **104**, 4271 (2004).
17. B. V. R. Choudari, G. V. Subba Rao, and S. Y. Chow, *Solid State Ionics*, **140**, 55 (2001).
18. H. J. Kweon, S. J. Kim, and D. G. Park, *J. Power Sources*, **88**, 255 (2000).
19. B. V. R. Choudari, G. V. Subba Rao, and S. Y. Chow, *J. Solid State Electrochem.*, **6**, 565 (2002).
20. H. Omada, T. Brousse, C. Marhic, and D. M. Schleich, *J. Electrochem. Soc.*, **151**, A922 (2004).
21. S. Al-Hallaj and J. R. Selman, *J. Power Sources*, **110**, 341 (2002).
22. P. Nelson, I. Bloom, K. Amine, and G. Henriksen, *J. Power Sources*, **110**, 437 (2002).
23. J. Kohler, H. Makihara, H. Uegaito, H. Inoue, and M. Toki, *Electrochim. Acta*, **46**, 59 (2000).
24. W. Li, J. R. Dahn, and D. Wainwright, *Science*, **264**, 1115 (1994).
25. M. Zhang and J. R. Dahn, *J. Electrochem. Soc.*, **143**, 2730 (1996).
26. C. H. Mi, X. G. Zhang, and H. L. Li, *J Electroanal. Chem.*, **602**, 245 (2007).
27. C. C. Chang, N. Scarr, and P. N. Kumta, *Solid State Ionics*, **112**, 329 (1998).
28. J. Cho and B. Park, *J. Power Sources*, **92**, 35 (2001).
29. C. H. Lu and H. C. Wang, *J. Mater. Chem.*, **13**, 428 (2003).
30. H. M. Wu, J. P. Tu, X. T. Chen, Y. F. Yuan, Y. Li, X. B. Zhao, and G. S. Cao, *J. Power Sources*, **159**, 291 (2006).
31. C. P. Fonseca, R. M. Paula, E. M. J. A. Pallone, and S. Neves, *Elcrochim. Acta*, **51**, 6419 (2006).
32. Y. Shao-Horn, S. Lavasseur, F. Weill, and C. Delmas, *J. Electrochem. Soc.*, **150**, A366 (2003).
33. A. J. Bard and L. R. Faulkner, *Electrochemical Methods: Fundamentals and Applications*, p. 242, 2nd ed. John Wiley & Sons, New York (2001).
34. Ali Eftekhari, *Elcrochim. Acta*, **47**, 495 (2001).
35. G. J. Wang, Q. T. Qu, B. Wang, Y. Shi, S. Tian, Y. P. Wu, and R. Holze, *Elcrochim. Acta*, **54**, 1199 (2009).
36. M. D. Levi, K. Gamolsky, D. Aurbach, U. Heider, and R. Oesten, *J Electroanal. Chem.*, **477**, 32 (1999).
37. M. D. Levi and D. Aurbach, *J. Solid State Electrochem.*, **11**, 1031 (2007).
38. J. Choi and A. Manthiram, *Electrochem. Solid State Lett.*, **7**, A365 (2004).
39. C. Ho, I. D. Raistriek, and R. A. Huggins, *J. Electrochem. Soc.*, **127**, 343 (1980).
40. B. Lin, Z. When, Z. Gu, and S. Huang, *J. Power Sources*, **175**, 564 (2008).
41. M. D. Levi and D. Aurbach, *J. Phys. Chem. B*, **101**, 4641 (1997).
42. M. D. Levi, G. Salitra, B. Markovsky, H. Teller, D. Aurbach, U. Heider, and L. Heider, *J. Electrochem. Soc.*, **146**, 1279 (1999).
43. B. Lin, Z. Wen, Z. Gu, and S. Huang, *J. Power Sources*, **175**, 564 (2008).